Design and Control of a Small-Clearance Driving Simulator — Source link ⧉

Lamri Nehaoua, Hakim Mohellebi, A. Amouri, Hichem Arioui ...+2 more authors

Institutions: University of Évry Val d'Essonne, Institut national de recherche sur les transports et leur sécurité, Centre national de la recherche scientifique

Topics: Driving simulator, Motion control, Steering wheel and Vehicle dynamics

Related papers:

- Simulator motion-drive algorithms - A designer's perspective

- An Optimal Control Approach to the Design of Moving Flight Simulators

- Motion cueing in the renault driving simulator

- Coordinated Adaptive Washout for Motion Simulators

- Motion Washout Filter Tuning: Rules and Requirements

Design and Control of a Small-Clearance Driving Simulator.

Lamri Nehaoua, Hakim Mohellebi, Ali Amouri, Hichem Arioui, Stéphane Espié, Abderrahmane Kheddar

Design and Control of a Small-Clearance Driving Simulator

Lamri Nehaoua, Hakim Mohellebi, Ali Amouri, Hichem Arioui, Stéphane Espié,
and Abderrahmane Kheddar, *Member, IEEE,*

Abstract— This paper presents a driving simulation which aim is twofold: (i) investigate the possibility to reduce motion clearance in order to achieve compact and low cost driving simulators, and (ii) evaluate multimodal and immersive virtual reality motion restitution in platooning driving. The choice has been made for a driving simulator having at least two degrees of freedom. These consist of the longitudinal displacement and seat rotations. The simulator is also equipped with force feedback steering wheel for virtual drive assistance. These components are gathered on a serial kinematics type platform in order to facilitate control scheme, and avoid the architecture complexity. A comparative study was made to devise a motion cueing strategy, taking into account both psychophysical and technological constraints. Experimentations were carried out for several cases combinations of longitudinal displacement and seat rotations.

Index Terms— Driving simulator, low clearance, motion cueing, psychophysics-based tuning

I. INTRODUCTION

DRIVING simulators have become useful tools for car designing, training, and driver's behavioral study. Their utility has interested several universities and industrial laboratories, for the development of new prototypes and validation of vehicle dynamic models. Nowadays, the important vehicles number and subsequent road traffic became very problematic and expensive in human lives. The increasing statistics of road accidents urged several governmental institutions to encourage the researchers in various fields of transport and vehicular design, to improve the road safety. Driving simulators make possible a better understanding of the human's behavior in drive situations close to reality.

Driving simulators became very accessible by technological headway. Indeed, the calculators become more powerful and less expensive. Thus, several simulators[1] of various architectures were built with an aim of either human factor study [1][2][3][4], or vehicle dynamic model validation, or test of new car prototypes and functionalities [5][6][7].

Researches were led to show the nearly dominant role 'vection' plays in human perception of motion [8]. These studies were exploited to some extent by the so called fixed-base simulators. In this case, the driver controls a set of driving commands such acceleration/deceleration, braking, steering,

[1]From now on, simulator is meant to designate driving simulator.

while perceiving visual feedback of the current situation. In order to allow the operator's virtual driving to be as close as to that of a real situation, it would be necessary to equip the simulator with equivalent multimodal cues (namely: visual, sound, haptic and inertial effects). Therefore, mobile platforms were combined with other displays to reproduce -in a reduced workspace- in best the sensations perceived in the real case. This way makes it possible to improve both immersion quality and simulation performances [9][10][11][12].

In such simulators, a large range of real-driving experienced accelerations cannot be reproduced. A compromise is to be found between the quality of various inertial indices' restitution and maintaining the platform within its reachable workspace. Therefore, many control strategies were developed. They were firstly used for flight simulators motion cueing. Their porting to vehicle simulators is possible, but the vehicle dynamics is of much higher frequencies (more abrupt and frequent acceleration variation) than what is observed on airplanes. Besides, driving a vehicle takes place within traffic and unforeseen events (fog, pedestrians...) conditions which could create more complex scenarios.

Motion cueing algorithms are based on three main principles. The first one consists in controlling the platform within its physical limits, according to what need to be fed back from the simulation engine. The second principle, commonly called washout, brings back carefully the platform toward its neutral position without causing sensory conflicts. Finally, the third principle, known as tilt-coordination, reproduces an illusory sustained accelerations by tilting with care the platform's cabin (i.e. in a way the driver do not perceive the tilting).

Three classes of motion cueing strategies were developed and detailed in the literature: classical, optimal and adaptive algorithms. The so called classical strategy, initially proposed by Schmidt and Conrad [13] to control the NASA's flight simulator, was implemented on the most of flight and driving simulators [14][15]. It consists in using a high-pass filter, to extract the transient component of the longitudinal acceleration. Filtered acceleration is then integrated twice to determine the platform desired displacement. Sustained longitudinal acceleration is extracted using a low-pass filter, and is reproduced by the tilt-coordination principle. The resulting tilt angle is added to that reproducing the angular velocities.

Adjustment of various algorithms requires psychophysical knowledge, and depends on (i) the simulator architecture, (ii) the carried out maneuver, and (iii) the virtual environment [16][17][18][19]. Hence, the classical approach, except its simplicity, suffers from some problems. It does not integrate

explicitly a perception model, and filter parameters tuning is done in the worst case (workspace is then not fully exploited during moderate acceleration or braking). To overcome these limitations, an approach that borrows from optimal control theory, including a perceptual model has been developed. Finally, an adaptive approach makes it possible to compute the filters' parameters at each time step, according to input acceleration or braking of the simulated vehicle.

In this paper, a low-cost motion platform having two degrees of freedom has been designed and built [20][21]. The choice of this architecture is motivated by two research investigations: how a low clearance can be coupled with rich complementary multimodal cues to allow compact and fully functional driving simulator? Is the system useful for driver's behavior study in platooning driving contexts? In the next section, the mechatronic architecture of the mini simulator SIM^2, and its modeling (longitudinal displacement and rotation of seat) are described. The third section justifies the choice of the motion cueing algorithm, which is assessed by qualitative and quantitative comparisons. Finally, experimental results, psychophysical evaluations and conclusions are given.

II. PLATFORM CONCEPTION

A. Simulator architecture

We aimed at devising a mini driving simulator that constitutes an acceptable compromise between: restitution quality, compactness, and cost constraints. The mechatronic components of the proposed solution are described below:

• *The cabin* consists of an instrumented mobile part moving along a guide-way mounted on the platform. It is the interface that lies between the driver and the simulation environment. The cabin is equipped with acceleration and braking pedals, steering wheel, gearbox lever and other classical car implements which are having appropriate sensors that allow the acquisition of the driver desired input commands (figure 1). These inputs feed the vehicle dynamic model to update its several states. The cabin disposes also of different visual indicators rendering the engine rpm, the vehicle speed, etc.

• *The acquisition system* is composed of an industrial microcontroller, and has both analog and digital input/output. This allows the control of the actuators in the desired position, speed or torque; this card appeared to be well adapted for the interfacing of the simulator's cabin. A bidirectional information exchange protocol is settled between this card and the PCs dedicated to vehicle-traffic model. This can be performed either through a parallel or an USB ports.

• *The vehicle model* concerns the computation of the dynamics and the kinematics according to the driver actions such as acceleration and brake pedals' positions, clutch... that are transmitted through the acquisition module and the road characteristics. It is a simple model dedicated to our simulator driving application. In this model, the vehicle is considered as one body with 5DOF (longitudinal, lateral, roll, pitch and yaw). Its complexity relates more to the motorization part than the chassis dynamic. The engine part is modeled by a mechanical and behavioral approaches [22] based on the vehicle general characteristics (engine torque curves, clutch

pedal position, accelerating proportioning, etc). After updating the vehicle's state, resulting information on the engine are sent to the cabin's dashboard and to the traffic model server.

• *The traffic model* is one of the most important parts of the simulation. It is the outcome of the ARCHISIM project [23] which provides a realistic simulation of road situations, starting from the individual drivers' behavior. ARCHISIM allows the simulation of road traffic of several tens of moved objects in real-time. Thus, it is possible to 'immerse' the driver in realistic traffic conditions.

• *The visual system* is based mainly on Silicon Graphics Inventor Performer library. The visual animated synthetic images are displayed on a wall either by three BARCO projectors and three adjacent screens giving a large visual field, or a PC solution using commercial video-projection.

• *The audio system* 3D sound restitution is based on Windows AEX library. During the driving simulation, the fed back sounds are composed mainly of those coming from the virtual vehicle (engine) and of the traffic environment. The virtual sound also enhances driver immersion.
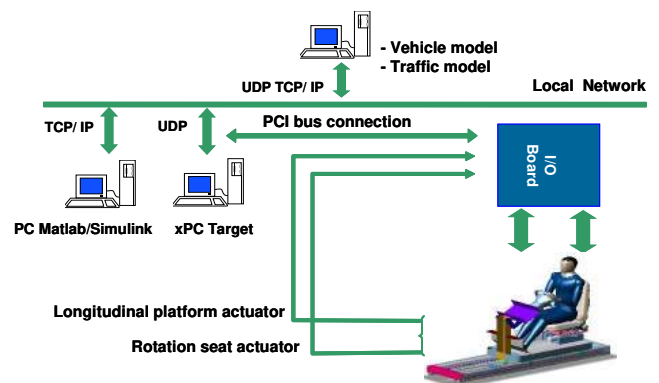

Fig. 1. Simulation Synoptic Architecture.

The platform is embedded with sensors and acquisition modules to have information feedback on the control system states. Each actuator has several sensors: angular position transducer (optical encoder), angular velocity (tachometer), and the output torque's sensor. Data resulting from these sensors are sent to the input/output interface board that is managed by a control PC. Actuators' power stage consists of a voltage servo-controller which receives a reference signal between 0–10Volts. According to this reference, the servo-controller modulates linearly the motor voltage input.

The control PC is managed by the xPC-Target. This tool has the advantage of being very flexible for prototyping and testing control algorithms on real systems. The different control algorithms are carried out on a standard target PC, while the Matlab/Simulink applications are sent from a host PC; they communicate via UDP (User Datagram Protocol). It is replaced by an embedded solution consisting in a microcontroller board with a CAN bus system interface for commercialization purpose.

B. Platform description

Our aim is to devise a small clearance platform for motion restitution and to search sufficient inertial effects that allows a similar driving behavior in virtual reality. We designed and achieved a low cost mobile platform equipped with three degrees of freedom (two of which are exclusive) and enough initial clearances for preliminary investigations. The first mobility translates the cabin front and rear longitudinal movement. The second mobility consists of rotating lightly either the seat or the seat's back -manual switch-, independently from the first.

1) Longitudinal platform conception: The platform carries both the cabin of the mini-simulator and the driver. By means of four sliders, assembled under the four ends of the cabin's base, the platform is able to move on a rail of 1.20m length. To this end, a Brushless type motor Parvex NX620 EAR is fixed at a mechanical stand related to the platform's rails. The motor rotation is transformed into cabin's longitudinal motion through a ball-screw-nut system (see figure 2). This platform achieves linear accelerations up to $\pm 0.66g$ in steady mode. At peak current, acceleration and speed of $\pm 1.32g$ and ± 3.95m/sec respectively are reached.
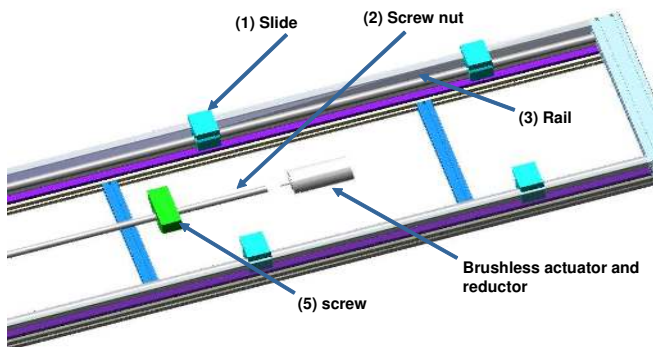

Fig. 2. Longitudinal platform mechanism.

Fig. 3. Under seat's mechanics.

2) Platform's seat conception: The mechanism of the seat is designed in order to realize small rotations up to ± 10deg of either the entire seat or only the seat's back. These two configurations are realized using a metal arm attached with the seat's back. This one comprises a groove in which a screw can slide. A second mechanical element, fixed under the seat's base, comprises a groove in the same axis as that of the first metal arm. Consequently, the screw can slide through the two grooves, either to fixes the metal arm at seat's base, or to disassociates it; this is illustrated in figure 3 which allows one to commute between the two configurations.

The different rotations are produced by a Brushless type motor Parvex RX320 fixed below the seat. A transmission system made up of a ball screw nut coupled to a pulley belt system transforms the rotational movement of the motor into translation of the nut fixed on a metal arm. This one being attached to the seat, it engenders finally a rotational motion of the seat and/or seat's back. In order to prevent the driving-shaft from deforming due to radial efforts, the motor frame can turn around an axis to realign the two axes of the nut and the screw.
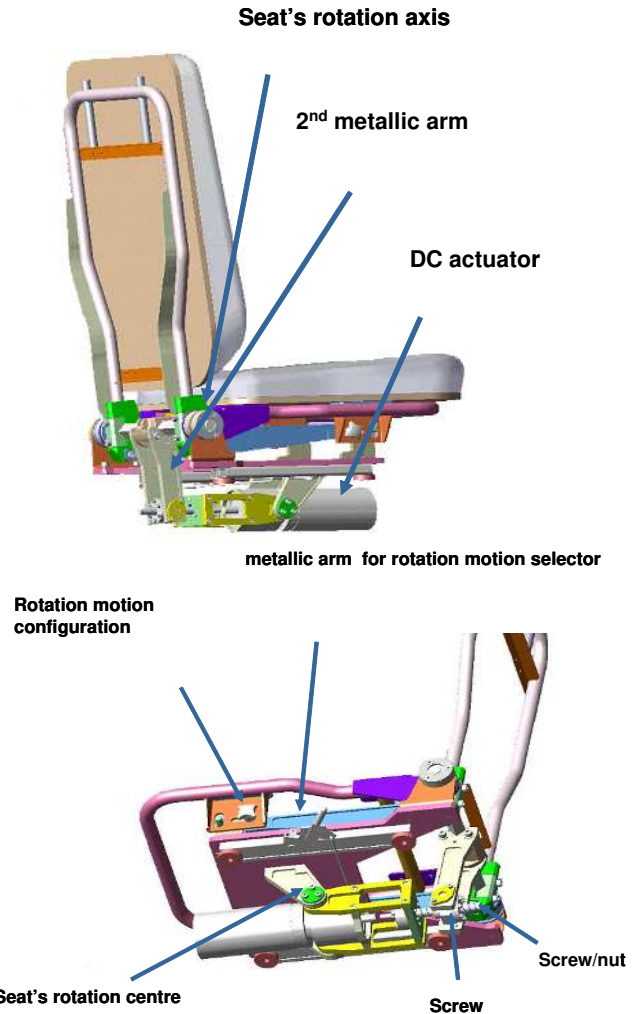
This system reproduces a linear acceleration of $\pm 0.127g$ at the driver vestibule. At peak current, a vestibule linear acceleration up to $\pm 0.662g$ is reached (the average distance between the seat's rotation axis and the driver's vestibule is ≈ 0.95m).

C. Haptic feedback steering wheel

To give an actual vehicle a desired course, the driver exerts efforts on the steering wheel. Efforts due to the tire/road contact and vehicle dynamics are also transmitted to the steering wheel through the steering column linkages. This perceived feedback is is necessary to orient well the vehicle and to feel the limits of its adherence. To allow haptic feedback we motorized the steering wheel of the cabin and developed our own algorithm inspired from teleoperation technology. Indeed the energy which flows between the driver and the vehicle front wheels through the mechanical linkage can be considered to be mainly effort and flow exchange corresponding to force and velocity [24]. Therefore, the cabin's steering system is modeled based on the principle of linear

quadripole formalism, in a similar way electrical networks are modeled. This technique proved to be efficient in the field of teleoperation and haptics [25]. Each element of the steering system will be represented by a chain matrix. Interconnection of all matrices (corresponding to their product) forms the final system (figure 4).
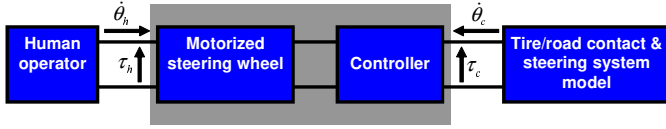

Fig. 4. Haptic feedback steering wheel.

The virtual tire/road computations are performed within the simulation process. Vehicle state, partially governed by the steering angle, and eventually the applied torque can be read in real-time by the simulation engine. A bilateral controller emulating both the mechanical linkage and the tire/road interaction is already functional. There is also a force feedback on pedals but it is not actively controlled; passive spring/damping mechanisms are used instead and can be tuned to behave closely to that of an actual vehicle.

D. Platform modeling

The overall system is considered as two independent subsystems linked mechanically: the rotating driving seat and the longitudinal motion platform. Each of them is driven by a single actuator and a screw nut device. The motion platform translates according to one direction (front and back) which corresponds to driver's deceleration and acceleration. A careful design and dimensioning allowed obtaining a simple linear model of the motion and achieve requirements in terms of accelerations to be reproduced, delivered torque, nominal rotational rates and thermal dissipation.

1) The longitudinal motion of platform: The motion base supports the cabin which consists of the seat, the vehicle chassis and the driver. Because the seat's rotations are slow and of low amplitude, its induced inertia is negligible comparing to the total mass of the cabin's set. The linear motion of the cabin's set is made thanks to a ball screw nut transmission mechanism driven by a DC actuator. The technological design was made in order to reduce: the mechanical flaws, the static and dynamic friction, and to facilitate the design of motion cueing controllers.

To model the dynamics of the longitudinal system, we firstly write the electrical equations of the Brushless DC actuator. The general actuator's electric equation is:

$$u_1 - e_1 = R_1 i + L_1 \frac{di_1}{dt} \tag{1}$$

where, u_1, e_1: armature and back electromotrice voltage (Volt). R_1, L_1: armature resistance (Ohm) and inductance (Henry) and i_1: armature current (Ampere).

The mechanical equation of the actuator pulling the platform's cabin is:

$$T_{a1} = J_{a1} \frac{d\omega_{a1}}{dt} + f_{a1}\omega_{a1} + \frac{T_{l1}}{N_1} \tag{2}$$

where, T_{a1}, T_{l1}: actuator and load torque (N.m). J_{a1}, f_{a1}: inertia (kg.m^2) and dynamic friction (N.m.sec/rad) of actuator's rotor. ω_{a1}: rotor's rotational velocity (rad/sec) and N_1: reduction ratio.

It is known that the torque T_{a1} relates to the armature current i_1, and the generated voltage relates to the shaft rotational velocity ω_{a1} and the back counter-electromotrice voltage e_1, that is:

$$T_{a1} = k_{t1}i_1 \quad \text{and} \quad e_1 = k_{e1}\omega_{a1} \tag{3}$$

where, k_{t1} and k_{e1}: actuator's constants.

We have now two components: the balls screw nut transmission mechanism and the cabin's set. The last is considered as a whole having a mass M sliding on a mechanical guide-way, which induces a friction f_{x1} during motion, under an external applied force F_{x1}. The entire cabin set sliding according to the $\vec{x}$ axis. The governing equation is:

$$M\ddot{x} + f_{x1}\dot{x} = F_{x1} \tag{4}$$

The balls screw nut pulling mechanism is driven by the external torque T_{s1}, indeed:

$$T_{s1} = J_{s1} \frac{d\omega_{s1}}{dt} + f_{s1}\omega_{s1} + T_{t1} \tag{5}$$

where, J_{s1}, f_{s1}: inertia and dynamic friction of the screw nut system. T_{t1}: screw nut load torque and ω_{s1}: rotational velocity of the screw nut.

Now, it is to link the three systems. Firstly, the pulling mechanism is linked to the cabin's set through the variables T_{t1} and F_{x1}. In fact, the load torque T_{t1} is transformed through the linkage to the axial force F_{x1} by the following equation:

$$T_{t1} = \frac{p_1}{2\pi\eta_1} F_{x1} \tag{6}$$

where, p_1 and η_1: tread (mm) and yield of the nut system.

Replacing equations (4) and (6) into (5) gives:

$$T_{s1} = J_{s1} \frac{d\omega_{s1}}{dt} + f_{s1}\omega_{s1} + \frac{p_1}{2\pi\eta_1} (M\ddot{x} + f_{x1}\dot{x}) \tag{7}$$

Linking the pulling balls screw nut mechanism to the actuator is made through the variables T_{s1} and T_{l1}. Indeed, the actuator load torque is, in fact, the applied screw nut torque, thus $T_{s1} = T_{l1}$, so equation (2) becomes:

$$\begin{aligned} T_{a1} &= J_{a1}\dot{\omega}_{a1} + f_{a1}\omega_{a1} + \frac{1}{N_1}[J_{s1}\dot{\omega}_{s1} + f_{s1}\omega_{s1} \\ &\quad + \frac{p_1}{2\pi\eta_1}(M\ddot{x} + f_{x1}\dot{x})] \end{aligned} \tag{8}$$

We can express this equation either in the cabin Cartesian space x or the actuator joint space ω_{a1} using:

$$\dot{x} = \frac{p_1}{2\pi}\omega_{s1} \tag{9}$$

and the one linking the actuator velocity to the screw nut pulling one through the reduction factor N_1, that is:

$$\omega_{s1} = \omega_{a1}/N_1 \tag{10}$$

Finally, replacing and rearranging the previous equations:

$$
\begin{aligned}
k_{t1} i_1 = & \underbrace{\left(\frac{2\pi N_1}{p_1} J_{a1} + \frac{2\pi}{p_1 N_1} J_{s1} + \frac{p_1}{2\pi \eta_1 N_1} M \right)}_{J_1} \ddot{x} + \\
& \underbrace{\left(\frac{2\pi N_1}{p_1} f_{a1} + \frac{2\pi}{p_1 N_1} f_{s1} + \frac{p_1}{2\pi \eta_1 N_1} f_{x1} \right)}_{f_1} \dot{x} \quad (11)
\end{aligned}
$$

Since:

$$
u_1 = R_1 i_1 + L_1 \frac{di_1}{dt} + \frac{2\pi N_1 k_{e1}}{p_1} \dot{x} \quad (12)
$$

and using the well known Laplace transform, we can obtain the transfer function between the cabin's position $X(s)$ and the voltage command signal $U_1(s)$ as:

$$
\frac{X}{U_1} = \frac{1}{s} \frac{k_{t1}}{\left[(J_1 s + f_1)(L_1 s + R_1) + \frac{2\pi N_1}{p_1} k_{e1} k_{t1} \right]} \quad (13)
$$

2) The rotating seat model: As stated previously, the driver seat can perform two kinds of small rotational motions: the rotation of only the seat's back or the rotation of the entire seat. This is achieved by a single actuator thanks to a manual switch. This motion can be coupled to the linear one giving five possible combinations for experimental investigations of motion cueing strategies:

- linear motion of the platform coupled to the entire seat rotation;
- linear motion of the platform coupled the only seat back's rotation;
- the platform linear motion alone;
- the entire seat's rotation alone;
- the entire seat back's rotation alone.

The seat system can be split into three sub-systems: the actuator set, the balls screw nut transmission mechanism, and the seat (including the driver). At the actuator level, the electric and mechanics equations are the same, and the different parameters are taken according to the new actuator and reduction factor. The balls screw nut pulling system is also similarly modeled. The load torque at the screw nut interaction level T_{t2} generates an axial force F_{t2}:

$$
T_{t2} = \frac{p_2}{2\pi \eta_2} F_{t2} \quad (14)
$$

The seat system parameters are variable because of driver's variability. Subsequently, it is difficult to determine the gravity center and the inertia parameters accurately. Nevertheless, we consider that the gravity center is located at a point G at a distance ρ from the rotation axis $\vec{y}$ of the seat. The balls screw nut axis is located at a distance l from the axis $\vec{y}$. Then, the applied forces at the seat (or seat's back) are the gravity force and the traction force F_{t2} of the screw nut.

First, we must compute the momentum of the system with respect to the rotation center of the seat. For this, we define two frame reference axes: the absolute reference $\Re_0 (O_0, \vec{x}_0, \vec{y}_0, \vec{z}_0)$ and the relative reference $\Re_1 (O_1, \vec{x}_1, \vec{y}_1, \vec{z}_1)$ related to the rotation center of the seat,
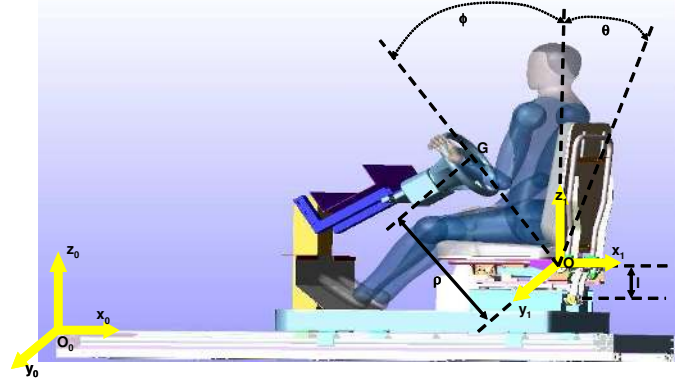

Fig. 5. Seat axis space and geometrical parameters.

as shown in figure 5. The dynamic momentum of the system seat-driver with respect to $\Re_1$ is:

$$
\vec{\delta}(O_1) = \vec{\delta}(G) + m_t \vec{\gamma}(G) \times \overrightarrow{GO_1} \quad (15)
$$

where, m_t: the whole seat and driver mass and $\vec{\gamma}(G)$: acceleration of the gravity center expressed as:

$$
\vec{\gamma}(G) = \frac{d^2 \overrightarrow{O_0 O_1}}{dt^2} + \frac{d\vec{\omega}}{dt} \times \overrightarrow{O_1 G} + \vec{\omega} \times \left(\vec{\omega} \times \overrightarrow{O_1 G} \right) \quad (16)
$$

where, $\vec{\omega} = \dot{\theta} \vec{y}_1$: is the seat rotation velocity. After rearranging the previous equations, we have:

$$
\vec{\gamma}(G) = \begin{cases} \ddot{x} + \ddot{\theta} \rho \cos(\theta + \varphi) - \dot{\theta}^2 \rho \sin(\theta + \varphi) \\ 0 \\ -\ddot{\theta} \rho \sin(\theta + \varphi) - \dot{\theta}^2 \rho \cos(\theta + \varphi) \end{cases} \quad (17)
$$

then, by neglecting the second order term $\dot{\theta}^2$:

$$
\vec{\delta}(O_1) = \left(J_{t2} \ddot{\theta} + m_t \left(\ddot{x} \rho \cos(\theta + \phi) + \ddot{\theta} \rho^2 \right) \right) \vec{y}_1 \quad (18)
$$

where, J_{t2}: the whole seat and driver mass, φ: angle between the line $O_1 G$ joining the gravity center G and the origin of the relative reference O_1 and the z_1 axis of the relative reference $\Re_1$ at the begining of the simulation.

Applying classical fundamental dynamics law to the seat system:

$$
m_t g \rho \sin(\theta + \phi) + F_{t2} l = J_{t2} \ddot{\theta} + m_t \left(\ddot{x} \rho \cos(\theta + \phi) + \ddot{\theta} \rho^2 \right) \quad (19)
$$

where, g: gravity vector.

Since the screw speed is related to the induced linear motion by $\omega_{s2} = \frac{2\pi}{p_2} \dot{x}$, and $x = l\theta$, then:

$$
\omega_{s2} = \frac{2\pi}{p_2} l \dot{\theta} \quad (20)
$$

Now, replacing each item, in a way similar to the motion platform modeling gives:

$$
k_{t2} i_2 = J_2 \ddot{\theta} + f_2 \dot{\theta} - \frac{p_2}{2\pi \eta_2 l N_2} m_t f(x, \theta) \quad (21)
$$

where:

$$f(x, \theta) = \ddot{x}\rho \cos(\theta + \phi) - g\rho \sin(\theta + \phi)$$
$$J_2 = \left(\frac{2\pi l N_2}{p_2} J_{a2} + \frac{2\pi l}{p_2 N_2} J_{s2} + \frac{p_2}{2\pi \eta_2 l N_2} \left(J_t + m_t \rho^2 \right) \right)$$
$$f_2 = \left(\frac{2\pi l N_2}{p_2} f_{a2} + \frac{2\pi l}{p_2 N_2} f_{s2} \right)$$

(22)

III. MOTION RESTITUTION

Obviously, the physical limits of the platform do not allow reproducing the full range of the inertial effects (accelerations). Moreover, we even seek to lower at maximum the longitudinal clearance of the platform. Thus, a cueing algorithm is necessary to generate platform trajectories which remain inside the reachable workspace while reproducing a driving behavior as close as to that of a real situation.

In this section we investigate three cueing algorithms (classical, optimal and adaptive) which are implemented and tested on the current simulator's platform. The goal here is to evaluate the different motion cueing algorithms and to choose the appropriate one for this driving simulator.
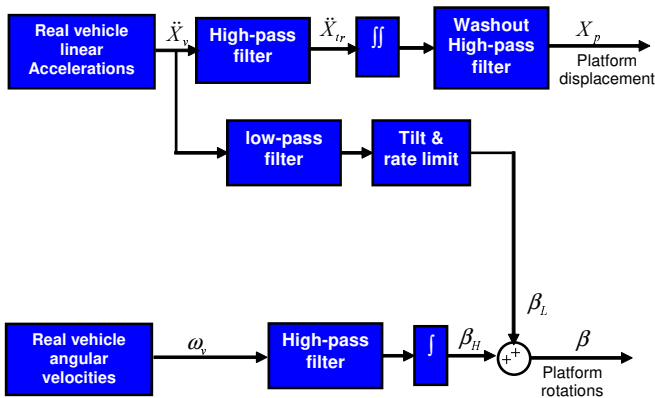
A. Classical Algorithm

Fig. 6. Motion cueing algorithm principle.

This algorithm consists of high-pass filtering the longitudinal acceleration resulting from vehicle dynamic model to extract its transient component. Filtered acceleration is integrated twice to have the desired platform's position. A low-pass filter extracts the sustained component of the acceleration used for tilt-coordination which uses gravity as an illusory sustained acceleration (figure 6). The Washout -consists in bringing back the platform to its neutral position- and tilt-coordination must be acheived with motions below the driver's perceivable threshold. Therefore, a precise comprehension on the vestibular system is required [26][27][28].

The filter order to be used is of importance because a high-pass filter should be at least of second order to limit the acceleration reference, and of third order to carry out a Washout. Generally, due to various model imperfections, the filters' parameters are tuned by a try-error heuristics. We propose a method which limits the interval of the parameters to be chosen (cut-off frequency, damping and static gain), while

taking into account the perception (thresholds) and actuators technology constraints (namely: time response and friction of actuators, absolute and relative maximum displacement allowed by the platform in response to a simulated acceleration over a time t_{max}).

We consider that the output of the Washout filter is the pulse response of a second order low-pass filter as follows [29]:

$$\frac{X_p(s)}{\ddot{X}_{tr}(s)} = \frac{K}{s^2 + 2\zeta\omega_n s + \omega_n^2}$$

(23)

where, $X_p(s)$: platform position, $\ddot{X}_{tr}(s)$: transitory acceleration ζ: damping coefficient, ω_n : filter natural pulsation and K : static gain. The pulse response of this filter for a damping ratio $\zeta > 1$ is given by:

$$h(t) = \frac{K}{\tau_1 - \tau_2} \left[\exp\left(-\frac{t}{\tau_1} \right) - \exp\left(-\frac{t}{\tau_2} \right) \right]$$

(24)

where,

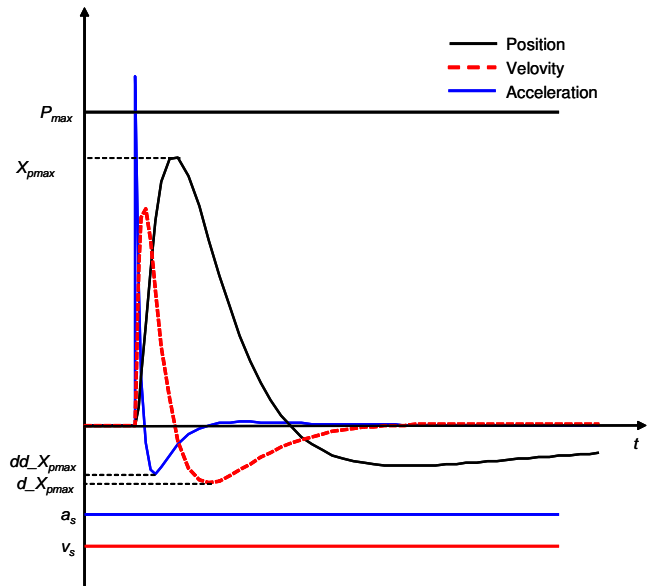$$\tau_{1,2} = \frac{\zeta}{\omega_n} \pm \frac{\sqrt{\zeta^2 - 1}}{\omega_n}$$

(25)

Fig. 7. Maximum position.

The choice of an over-damping coefficient ($\zeta > 1$) is made in order to eliminate false cues. From this equation, and its first, second and third derivatives, we deduce the maximum platform displacement, velocity and acceleration response values for a given transient acceleration input, indeed:
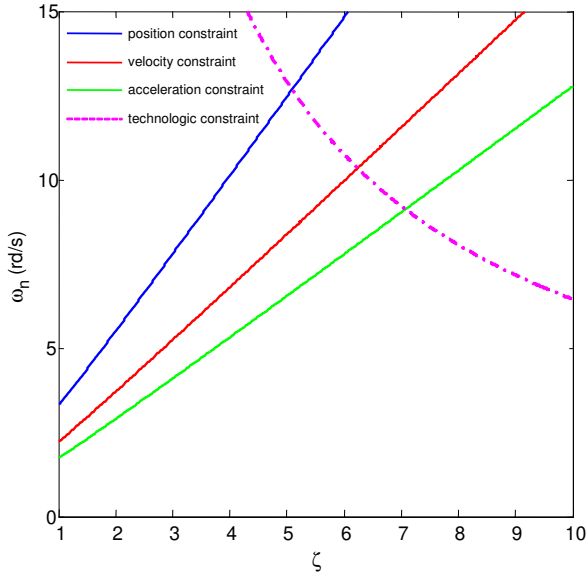
$$|X_{p\max}| = |K|\omega_n\xi < P_{\max}$$

(26)

$$\dot{X}_{p\max} = K\omega_n^2\xi^2 < v_s$$

(27)

$$\ddot{X}_{p\max} = K\omega_n^3\xi^3 < a_s$$

(28)

where,

$$\xi = \exp\left[\frac{\zeta}{\sqrt{\zeta^2 - 1}} \ln\left(\zeta - \sqrt{\zeta^2 - 1} \right) \right]$$

(29)

Fig. 8.   Acceptable parameters ζ and ω_n.

and $P_{\max}$ is the maximum allowed platform displacement ($P_{\min} = -P_{\max}$), v_s and a_s are the velocity and the acceleration thresholds of the vestibular system respectively (figure 7).

The technological constraint relates to friction, and consequently, its direct dependence of the actuator parameters and the Washout filter (these two blocks are assembled in cascade). Precisely, to benefit of the maximum of the actuator's characteristics (synthesized during initial dimensioning), the Washout filter must be selected in a manner to minimize the total friction. Therefore, a sufficient condition:

$$2\zeta\omega_n < f_0 \tag{30}$$

where, f_0: is the proper friction of actuation system, can achieve the matter. If this condition is not satisfied, the simulation depends only on the actuator's parameters, and consequently, the adjustment of the motion cueing algorithm would be reduced even eliminated. Shaded region in figure 8 presents the acceptable high-pass filter parameters (ω_n, ζ) which respect the constraints mentioned above.

B. Optimal algorithm

Initially proposed by Sivan et al. [30], it has been developed by Telban and Cardullo [31][32] to target an implementation on UTAIS flight simulator UTAIS. This algorithm uses filters of higher order with an optimization method borrowed from optimal control theory.

The distinguishing feature is in incorporating a mathematical model of the human vestibular system [33][34], in order to reduce the error between the vestibular system's output of the driver on the simulated vehicle and its counterpart coming from the driver on the driver simulator (figure 9).

The aim of this algorithm is to calculate a transfer function $W(s)$ which expresses the dynamic states of the simulator u_s
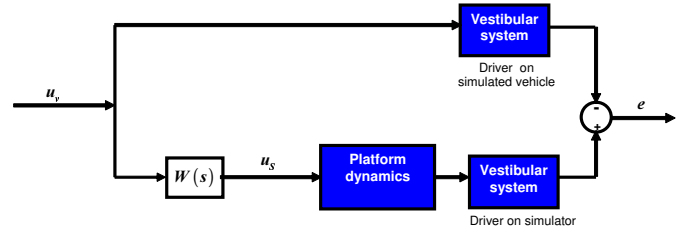

Fig. 9.   Optimal Washout scheme.

with respect to those of the simulated vehicle u_v

$$U_s(s) = W(s)U_v(s) \tag{31}$$

The optimal strategy determines the simulator acceleration u_s by minimizing a cost function of the form:

$$J(u_s) = E\left\{\int_0^\infty \left(e^T Q e + x_d^T R_d x_d + u_s^T R u_s\right) dt\right\} \tag{32}$$

where, e is supposed to be the sensory error, x_d is the state vector containing the platform's position and velocity, u_s is the platform's longitudinal acceleration. Q, R_d and R are weighting positive definite matrices; they define the compromise between the sensory error minimization and platform's physical constraints. Considering the small workspace of the platform and for security reasons, we have opted for restrictive position cost function. Figures 10, 11 and 12 show the comparison between optimal and classical algorithms for a square longitudinal acceleration; both cases with and without platform tilt-coordination.

C. Adaptive Algorithm

Firstly proposed by Parrish et al. [35] to provide motion cues for the Langley flight simulator. This algorithm can be seen as a classical one where parameters are variable and computed at each time step of simulation. Several variants were proposed to improve the stability of the algorithm [36], e.g. by including the vestibular model for the lateral false cues reduction [37].

It is based on the minimization of a cost function containing the acceleration error and constraints on the platform displacement. The adaptation is carried out using the steepest descent method to resolve the sensitivity equations. The resulting filter is then nonlinear (figure 13).

The filter equation is given by:

$$\ddot{x}_s = K\ddot{x}_v - 2\zeta\omega_n\dot{x}_s - \omega_n^2 x_s \tag{33}$$

where, $\ddot{x}_v$ is the simulated vehicle acceleration, $\ddot{x}_s, \dot{x}_s$, and x_s are the acceleration, the velocity and the position of the platform respectively. K, ζ, ω_n are the adapted Washout filter parameters. The cost function J to be minimized is:

$$\frac{1}{2}\left[w_a\left(\ddot{x}_v - \ddot{x}_s\right)^2 + w_v\dot{x}_s^2 + w_v x_s^2 + w_K\left(K - K_0\right)^2 + \right.$$
$$\left. w_\zeta\left(\zeta - \zeta_0\right)^2 + w_{\omega_n}\left(\omega_n - \omega_{n0}\right)^2\right] \tag{34}$$
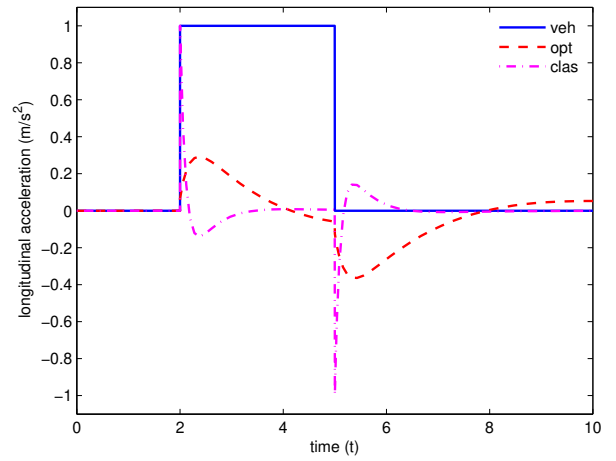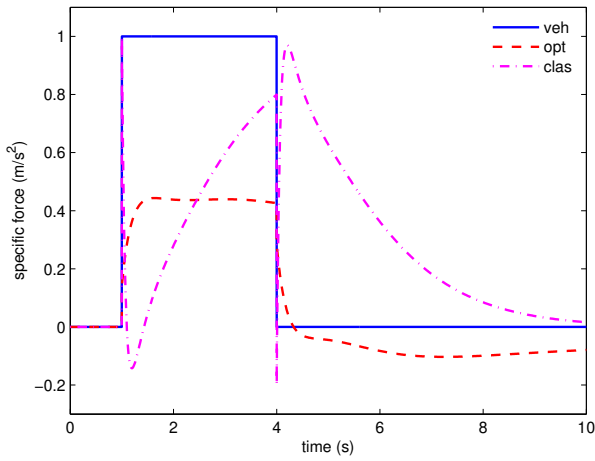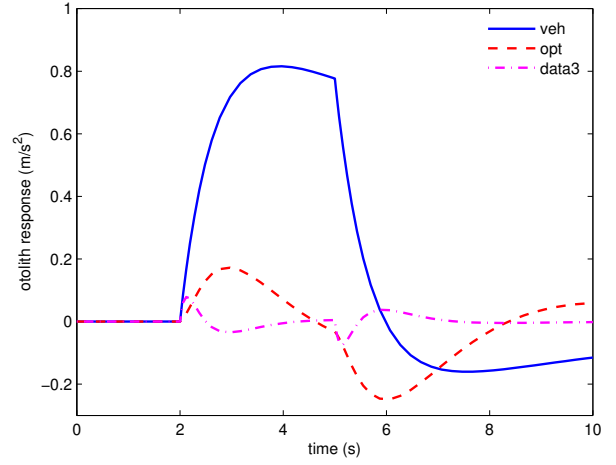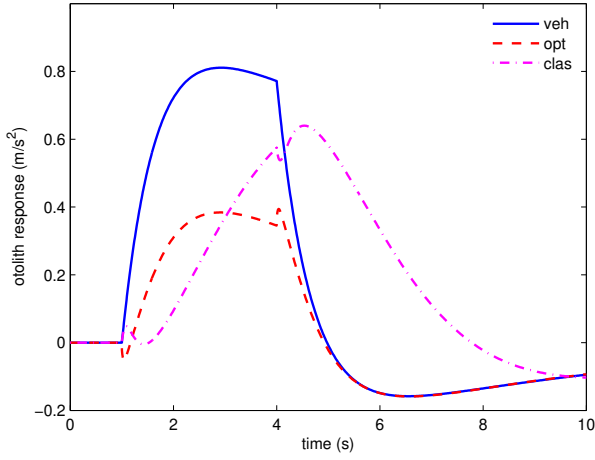
Fig. 10.   Otolith and specific force response comparison between optimal and classical algorithms with the platform tilt-coordination.

Fig. 12.   Otolith and specific force response comparison between optimal and classical algorithms with only the longitudinal platform motion.
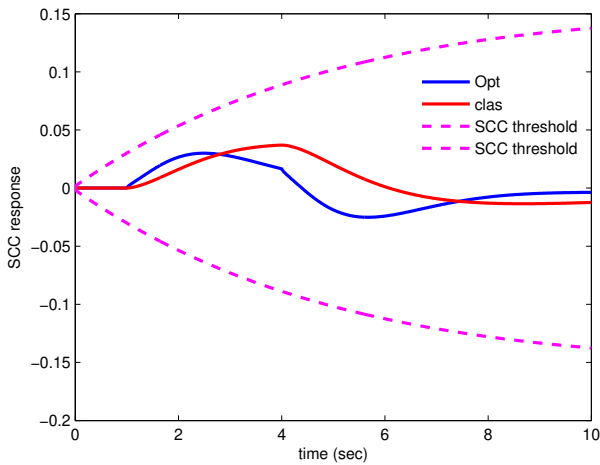

Fig. 11.   Semi-Circular Channels response comparison according to the tilt-coordination angular rate using optimal and classic algorithms.

Fig. 13.   Adaptive Washout algorithm.

Using the gradient descent optimization method [38]:

$$\dot{K} = -\gamma_K \frac{\partial J}{\partial K} \qquad (35)$$

$$\dot{\zeta} = -\gamma_\zeta \frac{\partial J}{\partial \zeta} \qquad (36)$$

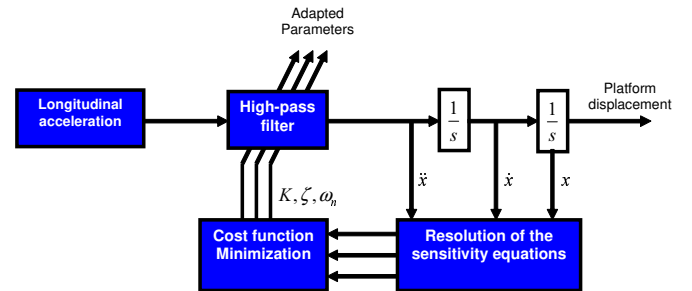$$\dot{\omega}_n = -\gamma_{\omega_n} \frac{\partial J}{\partial \omega_n} \qquad (37)$$

Once the weighting coefficients w_i of the cost function and the initial conditions K_0, ζ_0 and ω_{n0} are determined, the resolution of the sensitivity equations allows to have the acceleration and position signals to drive the platform. Figure 14 shows the comparison between adaptive and classical algorithms for a square longitudinal acceleration, in both case with and without platform tilt-coordination.
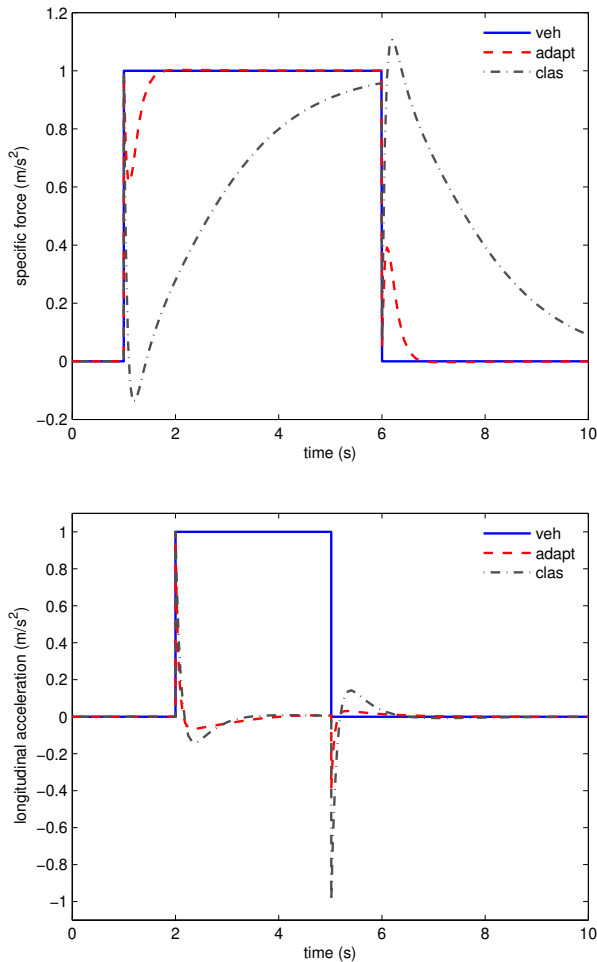
driving, during an acceleration or braking maneuvers and because of the inertial delay effect, the driver's bust rock in the reverse direction of the acceleration. Thus, we are interesting to compute the seat angular acceleration which affects the driver's bust. By a similar modeling approach as described in section II.C.2, we obtain the angular acceleration of the seat and driver system, as:

$$\ddot{\theta} = \frac{m_t g \rho \sin(\phi + \theta) - m_t \ddot{x} \rho \cos(\phi + \theta)}{J_t + m_t \rho^2} \quad (38)$$

By analyzing this equation, one distinguishes between the gravity effect in the one hand and the vehicle's acceleration effect on the other hand. We are interested only by the vehicle's acceleration, so we can extract it easily from the above equation, that is:

$$\ddot{\theta}_v = -\frac{m_t \ddot{x} \rho \cos(\phi + \theta)}{J_t + m_t \rho^2} \quad (39)$$

Based on this equation we are able to compute the angular acceleration that acts on the driver's bust. With the use of a classical motion cueing algorithm, we can restitute this acceleration by tilting the cabin's seat.

Fig. 14. Adaptive and classical Washout response comparison with (up) and without (down) tilt-coordination.

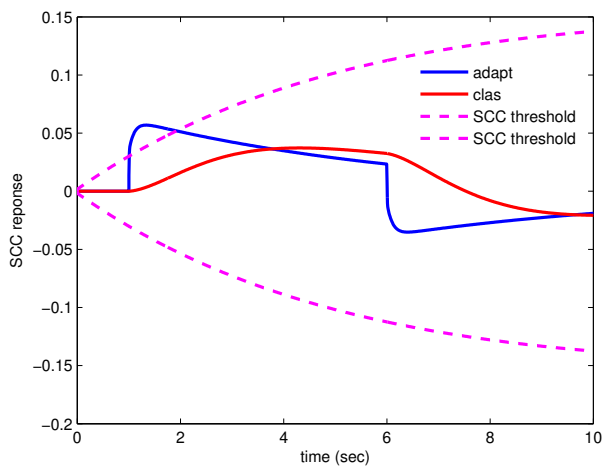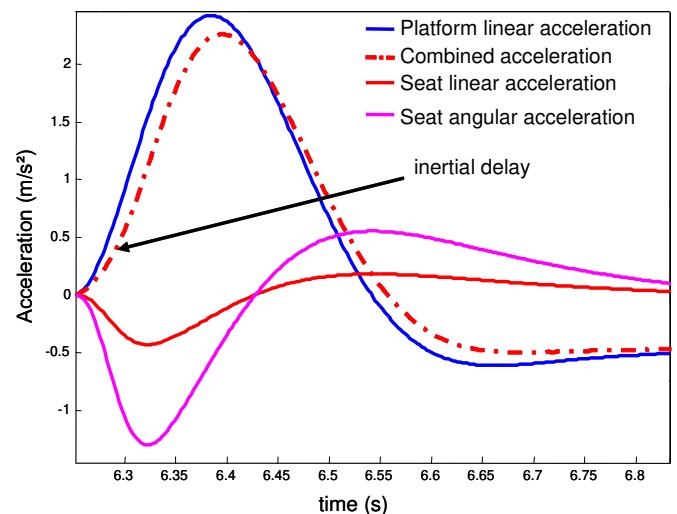Fig. 16. Restitution acceleration on the driver's bust for a linear longitudinal acceleration of the platform.

Fig. 15. Semi-Circular Channels response comparison according to the tilt-coordination angular rate using adaptive and classic algorithms.

D. Seat motion restitution

The seat was designed to feedback inertial effect that vehicle accelerations cause on the driver bust. Indeed, at real vehicle

Figure 16 illustrates the fed back accelerations on the driver's bust, during a longitudinal platform acceleration of 3m/sec^2. The seat's linear acceleration occurs in the opposite direction of the vehicle acceleration. Moreover, it is being applied to the bust of the driver by superposition (i.e. at the same time) to the platform acceleration. Then, the bust is subjected to the difference in two accelerations. Thus, the perception of continuous accelerations is delayed until the difference of the two accelerations exceeds the vestibular perception threshold. Also, the driver perceives the angular acceleration which moves the seat in the direction opposed to that of the platform movement.

IV. Experimental Results

A. Motion cueing algorithms

In order to compare the performances of previous described algorithms, experimentations were carried out on the presented driving simulator (figure 17).

Fig. 17. INRETS/IBISC SIM^2 mini driving simulator: the complete actual set-up in action.

Firstly, a scenario consisting in a set of accelerations, decelerations and braking maneuvers is accomplished (the signals are real ones, given by a car company). The resulting signals from the vehicle dynamic model is saved to be executed on the simulator for classical, adaptive and optimal algorithms. This is done to compare the different algorithms for the same maneuver. Parameters of each algorithm are adjusted to respect the physical constraints of the platform ($\pm 0.6m$) [39]. The platform's longitudinal acceleration and position are saved and plotted using Matlab/Simulink software to be analyzed.
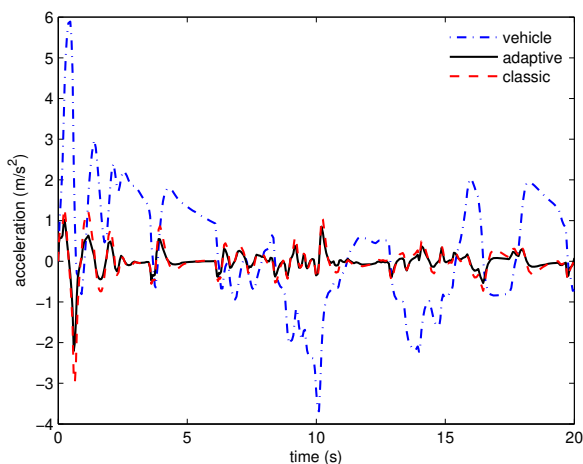

Fig. 18. Acceleration response comparison according to classical and adaptive algorithm.s

In absence of tilt-coordination, as the case of our platform, the classical and the adaptive algorithm show close performances. The restituted acceleration is better with a classical
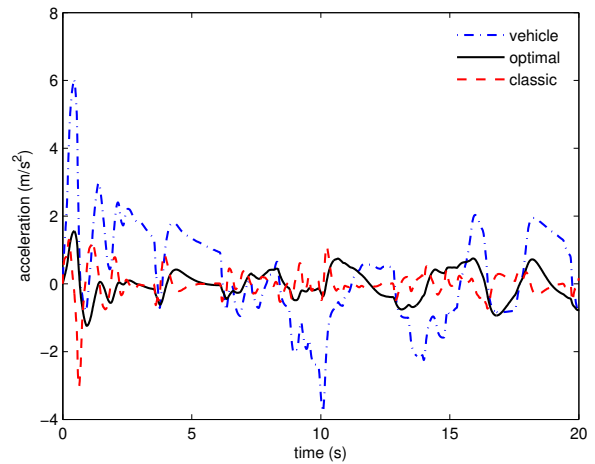

Fig. 19. Acceleration response comparison according to classical and optimal algorithms.
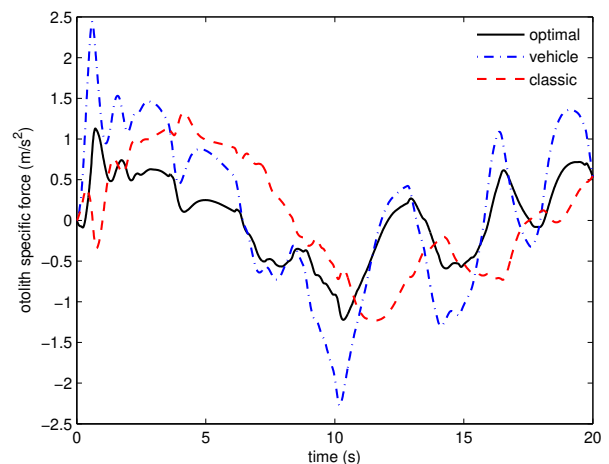

Fig. 20. Otolith specific force response comparison according to classical and optimal algorithms.

algorithm especially for acceleration phases, except that, with an adaptive gain, some false cues generated by the linear propriety of the high-pass filters are reduced (figure 18). In addition, Figure 21 shows that the Washout is few more quick with a classical algorithm than the adaptive one, and no considerable improvement in the platform workspace is done. Therefore, we can deduce that with just a longitudinal motion, even with an adaptive gain the classical algortihm presents a minor better performance comparing to the adaptive, with the advantage of a simple parameters tuning.

Optimal algorithm provides a better acceleration cueing, especially for onset acceleration and abrupt braking (figure 19). Its otolith response is the closest to the real situation compared to the classical and adaptive Washout filters, since it integrates a vestibular model in the cost function optimisation (figure 20). However, the Washout is very slow comparing to the calssical algorithm, which means that the optimal algorithm requires a larger workspace (figure 22) to be an interesting solution.
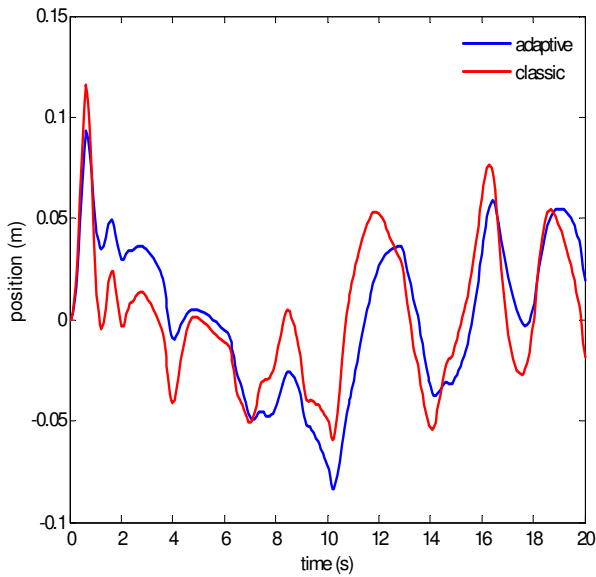
Fig. 21.   Position response comparison according to classical and adaptive algorithms.
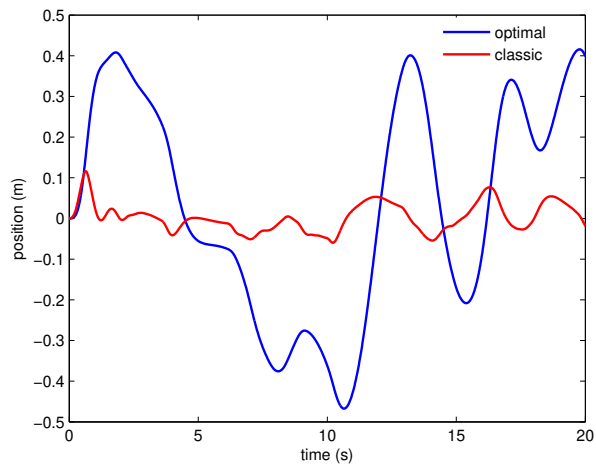

Fig. 22.   Position response comparison according to classical and optimal algorithms.

These results are very logic for two reasons. Firstly, with no tilt-coordination of the motion cueing algorithms, only the transitory accelerations are restituted. Secondly, the present platform is designed and dimensioned to explore the platooning driving situation, which presents moderate maneuvers.

Finally, due to tuning simplicity and algorithm rapidity, we have retained the classical strategy, associated with some artifacts (anti backlash algorithm [27], acceleration and braking pedals threshold detection) for the evaluation experiment.

B. Experimental Conditions

Six movement conditions have been proposed for the platform motion:
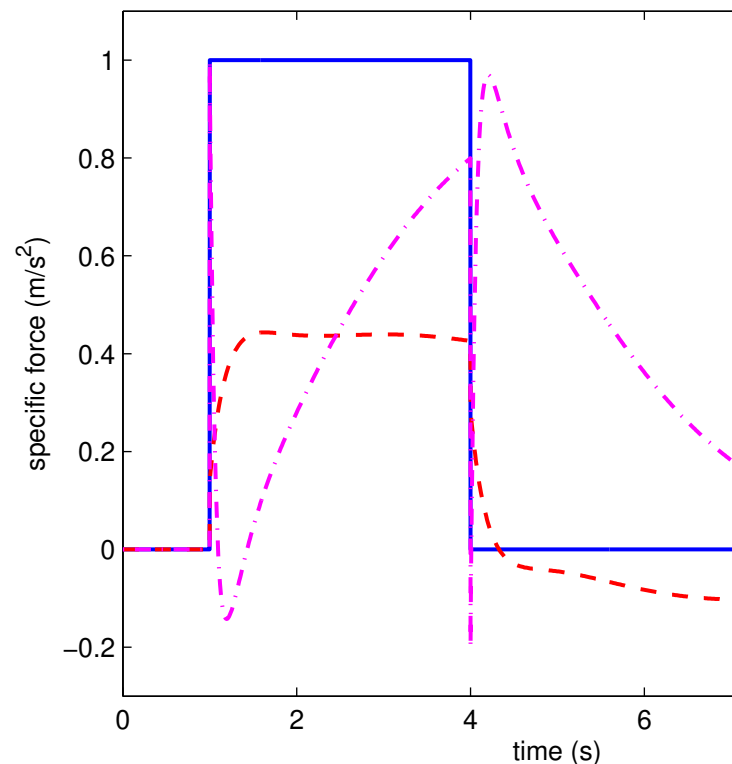
- Without movement (W-Off): no movement is activated on the platform (only visual feedback)
- Long platform movement (L-Off): only longitudinal movement is activated. The displacement and the maximum acceleration of the platform are $\pm 30cm$ and $\pm 0.4g$ respectively.
- Short platform movement (S-Off): only longitudinal movement is activated. The displacement and the maximum acceleration of the platform are $\pm 10cm$ and $\pm 0.2g$ respectively.
- Seat movement (W-On): only the seat rotation is activated.
- Long platform movement combined with seat movement (L-On): platform and seat movement are activated.
- Long platform movement combined with seat movement (S-On): platform and seat movement are activated.

C. Driving Simulator

Thirty two people participated to the experiment, they drove in a moving-base driving simulator SIM^2, with dynamic and interactive visual image. The drivers habits related to the driving activity were investigated by Manchester Driving Behavior Questionnaire (MDBQ). The main subjective dependant variables recorded was the rank allocated to each condition. We also considered the driver's comments as regards the realism of deceleration, acceleration and braking maneuvers. The objective dependent variables recorded were the mean headway time (HT) and the variation of decelerations (VARdec).

HT indication refers to the delay between the lead and the piloted vehicle. VARdec indication refers to the changes of deceleration of the piloted vehicle.

D. Results

The detailed psychophysics results of these experiments deserved a separate publication to which interested readers may refer [40]. The conclusion of this study are reported in this section. The main objectives of this research was, firstly, to assess the relevance of our driving simulator architecture choice (longitudinal and back of seat motion), and to compare different modalities for longitudinal accelerations rendering, and secondly, to support the use of individual characteristic measures as potential indices for the assessment of new driving simulators. It appears that the longitudinal displacement of the motion-base alone is not sufficient to modulate the driving performances in comparison to the lack of platform motion. However the tilt of the seat back coupled to longitudinal movement provides information that modulates them. The HT indication in S-On condition had decreased significantly regarding the other situations conditions. We can interpret this result as an increase of confidence and may be as an increase of the virtual vehicle control. We also remind that this condition is subjectively considered as the better among the six experimental conditions proposed in our experiment. Such interpretation is reinforced by the fact that the MDBQ individual parameter offers a same kind of result, but for prudent drivers exclusively.

V. CONCLUSION

Considering perceptual issues in driving a vehicle, we proposed a reduced clearance and low cost mobile platform which kept acceptable driving behavior and realism. Although these devices allowed partial restitution of dynamics inertial effects, dominant pertinent cue have been taken into account and displayed with appropriate stimuli combination which appear to be sufficient to carry out a behavioral plausible driving simulation.

The designed platform has two degrees of freedom. The first one makes it possible to drive the cabin of the simulator in a front/rear translation. The second makes possible to produce seat rotations. The combination of the two movements (translation and seat rotation) may give the illusion of acceleration variation. To animate the platform according to simulated vehicle accelerations, we studied and compared several motion cueing strategies (classical, optimal and adaptive) that we adapted and tuned to our hardware.

In order to identify the minimal inertial effect to achieve good performances on the control of longitudinal accelerations, a psychophysical evaluation has been conducted. It explored the various combinations movements accessible by the platform. For this evaluation, subjective and objective measurements were recorded. After data analysis reported in [40], the seat back rotation combined to small platform translations, seem to be the most appreciated combination.

In the perspective to expand field of simulator's application beyond the platooning drive scenarios, we are envisaging the integration of a third degree of freedom into the mobile platform.

REFERENCES

[1] P. Grant, B. Artz, J. Greenberg, and L. Cathey, "Motion Characteristics of the VIRTTEX Motion System," in *Proceedings of the 1st Human-Centered Transportation Simulation Conference*, IOWA, USA, 2001.

[2] L. D. Chen, Y. Papelis, G. Waston, and D. Solis, "NADS at the University of IOWA: A tool for driving safety research," in *Proceedings of the 1st Human-Centered Transportation Simulation Conference*, IOWA, USA, 2001.

[3] G. Reymond and A. Kemeny, "Motion cueing in the RENAULT driving simulator," in *Vehicule System Dynamic*, vol. 34, Paris, France, Oct. 2000, pp. 249–259.

[4] L. Sung, K. Ha, C. H. Cho, and L. J. Lee, "The KOOKMIN University Driving Simulators for Vehicle Control System Development and Human Factor Study," in *Driving Simulation Conference (DSC04)*, Paris, France, 2004.

[5] G. Reymond, A. Heidet, M. Canry, and A. Kemeny, "Validation of RENAULT's Dynamic Simulator for Adaptive Cruise Control Experiments," in *Proceedings of the Driving Simulator Conference (DSC00)*, Paris, France, 2000, pp. 181–191.

[6] M. Dagdelen, G. Reymond, A. Kemeny, and M. Bordier, "MPC based motion cueing algorithm: development and application to the ULTIMATE driving simulator," in *Proceedings of the Driving Simulator Conference (DSC04)*, Paris, France, 2004.

[7] D. Stall and S. Bourne, "The National Advanced Driving Simulator: Potential applications to ITS and AHS research," in *Proceeding of the 6th Annual meeting of the Intelligent Transportation Society*, Washington D.C, USA, 1996, pp. 700–710.

[8] A. Kemeny, "Simulation et perception du mouvement," in *Driving Simulation Conference (DSC99)*, Paris, France, July 1999, pp. 33–55.

[9] J. Freeman, G. Watson, Y. Papelis, T. Lin, A. Tayyab, R. Romano, and J. Kuhl, "The IOWA driving simulator : an implementation and application overview," in *SAE Technical Paper Series, No 950174*, Feb. 1995.

[10] J. Kim, W. Lee, L. Park, K. Park, and J. Cho, "A Design and Characteristic Analysis of the Motion Base for Vehicle Driving Simulator," in *IEEE International Workshop on Robot and Human Communication (ROMAN97)*, Paris, France, 1997, pp. 290–294.

[11] K. Tu, T. Wu, and T. Lee, "A study of Stewart platform specifications for motion cueing systems," in *IEEE International Conference on Systems, Man and Cybernetics*, 2004, pp. 3950–3955.

[12] S. Advani, M. Nahon, N. Haeck, and J. Albronda, "Optimization of Six-Degrees-of-Freedom Motion Systems for Flight Simulators," in *Journal of Aircraft*, vol. 36, Sept.-Oct. 1999, pp. 819–826.

[13] S. F. Schmidt and B. Conrad, "Motion drive signals for piloted flight simulators," in *Contractor Report NASA CR-1601*, Washington, USA, 1970.

[14] R. Parrish, J. Dieudonne, and D. Martin, "Motion software for a synergistic six degree of freedom motion base," in *NASA Technical Note D-7350*, Dec. 1973.

[15] M. McCauley, T. Sharkey, J. Sinacori, S. LaForce, J. Miller, and A. Cook, "A demonstration of motion base design alternatives for the National Advanced Driving Simulator," in *NASA Technical Memorandum 103881*, Oct. 1992.

[16] P. R. Grant and L. D. Reid, "Motion Washout Filter Tuning: Rules and Requirements," *Journal of Aircraft*, vol. 34, pp. 145–151, Mar.-Apr. 1997.

[17] M. A. Nahon and L. D. Reid, "Simulator Motion-Drive Algorithms: A Designer's Perspective," *Journal of Guidance and Dynamics*, vol. 13, pp. 356–362, July 1989.

[18] M. Idan and M. A. Nahon, "Off-Line Comparison of Classical and Robust Flight Simulator Motion Control," *Journal of Guidance and Dynamics*, vol. 22, pp. 702–709, Sept.-Oct. 1999.

[19] L. Reid and M. Nahon, "Response of Airline Pilots to Variations in Flight Simulator Motion Algorithms," in *Journal of Aircraft*, vol. 25, July 1988, pp. 639–646.

[20] H. Mohellebi, S. Espié, H. Arioui, A. Amouri, and A. Kheddar, "Low cost motion platform for driving simulator," in *5th International Conference on Machine Automation (ICMA04)*, Osaka, Japan, Nov. 2004.

[21] L. Nehaoua, A. Amouri, and H.Arioui, "Classic and Adaptive Washout Comparaison for a Low Cost Driving Simulator," in *Proceedings of the 13th Mediterranean Conference on Control and Automation (MED05)*, Limassol, Cyprus, June 2005, pp. 586–591.

[22] S. Marchant, "Réalisation d'un simulateur automobile," in *Master Thesis*, Ecole Nationale de l'Aviation Civile, France, Aug. 1995.

[23] S. Espie, "Vehicle-driven simulator versus traffic-driven simulator: the INRETS approach," in *Driving Simulation Conference (DSC99)*, Paris, France, June 1999, pp. 367–376.

[24] H. Mohellebi, S. Espié, and A. Kheddar, "Adaptive haptic steering wheel for driving simulators," in *Proceedings of 2004 IEEE/RSJ International Conference on Robots and Intelligent Systems (IROS04)*, June 2004.

[25] A. Kheddar and P. Coiffet, "Téléopration et Télérobotique," in *Edition Hermés*, Paris, 2002.

[26] J. L. Meiry, "The Vestibular System and Human Dynamic Space Orientation," in *M.I.T PhD Thesis*, Cambridge, Massachusetts, June 1965.

[27] G. Reymond, "Contribution respective des stimuli visuels, vestibulaires et proprioceptifs dans la perception du mouvement du conducteur," in *PhD Thesis*, University of Paris6, France, Dec. 2000.

[28] L. Harris, M. Jenkin, D. Zikovitz, and F. Redlick, "Simulating Self-Motion I: Cues for the Perception of Motion," in *Springer-Verlag Virtual Reality*, vol. 6, Sept. 2002, pp. 75–85.

[29] L. Nehaoua, H. Arioui, H. Mohellebi, and S. Espié, "Restitution Movement for a Low Cost Driving Simulator," in *Proceedings of the 2006 American Control Conference (ACC06)*, Minneapolis, Minnesota, June 2006, pp. 2599–2604.

[30] R. Sivan, J. Ish-shalom, and J. . Huang., "An optimal control approach to the design of moving flight simulators," *IEEE Transactions on Systems, Man and Cybernetic*, vol. 12, pp. 818–827, July-Aug. 1982.

[31] F. Cardullo, R. Telban, and J. Houck, "Motion cueing algorithms: A human centered approach," in *5th International Symposium on Aeronautical Sciences*, Zhukovsky, Russia, 1999.

[32] R. Telban and F. Cardullo, "A nonlinear human centred approach to motion cueing with neurocomputing solver," in *AIAA Modeling and Simulation Technologies Conference and exhibit*, Monterey, California, Aug. 2002.

[33] L. Young and J. L. Meiry, "A Revised Dynamic Otolith Model," in *Aerospace Medicine*, vol. 39, June 1968, pp. 606–608.

[34] R. Telban, F. Cardullo, and L. Guo, "Investigation of mathematical models of otolith organs for human centered motion cueing algorithms," in *AIAA Modeling and Simulation Technologies Conference*, Denver, USA, Aug. 2000.

[35] R. V. Parrish, J. E. Dieudonne, R. L. Bowles, and D. J. Martin, "Coordinated Adaptive Washout for Motion Simulators," *Journal of Aircraft*, vol. 12, pp. 44–50, July 1975.

[36] M. A. Nahon, L. D. Reid, and J. Kirdeikist, "Adaptive simulator motion software with supervisory control," *Journal of Guidance and Dynamics*, vol. 15, pp. 376–383, Mar.-Apr. 1992.

[37] D. Ariel and R. Sivan, "False cue reduction in moving flight simulators," *IEEE Transactions on Systems, Man and Cybernetic*, vol. 14, pp. 665–671, July-Aug. 1984.

[38] P. A. Ioannou and J. Sun, *Robust Adaptive Control*. Prentice-Hall Inc, 1995.

[39] L. Nehaoua, H. Arioui, H. Mohellebi, and S. Espié, "Motion Cueing Algorithms for Small Driving Simulator," in *Proceedings 2006 IEEE International Conference In Robotics and Automation (ICRA06)*, Orlando, Florida, May 2006, pp. 3189–3194.

[40] J. Neimer, H. Mohellebi, S. Espié, and A. Kheddar, "Optimization of linear motion base dedicated to normal driving conditions," in *Driving Simulator Conference (DSC05)*, Orlando, Florida, 30 nov-2 dec 2005.

VI. APPENDIX

A. PARVEX actuators's parameters

NX620: $R_1 = 2.47\Omega$, $L_1 = 19.2$mH, $J_{a1} = 98E - 5$kg.m^2, $f_{a1} \approx 0$, $N_1 = 1$, $k_{t1} = 1.07$N.m/A, $k_{e1} = 135$V/rpm.

RX320: $R_2 = 0.56\Omega$, $L_2 = 5.3$mH, $J_{a2} = 0.0005$kg.m^2, $f_{a2} = 0.05$N.m, $N_2 = 5$, $k_{t2} = 0.145$N.m/A, $k_{e2} = 15.2$V/rpm.

B. Screw-nut systems parameters

Platform: $J_{s1} = 17E - 5$kg.m^2, $f_{s1} = 0.0405$N.m, $p_1 = 0.025$m, $\eta_1 = 90\%$, $M = 180$kg, $f_{x1} = 0.1$N.m.

Seat: $J_{s2} = 0.626E - 5$kg.m^2, $J_{t2} = 17.71$kg.m^2, $f_{s2} = 0.05$N.m, $p_2 = 0.005$m, $\eta_2 = 80\%$, $M_t = 90$kg, $l = 0.16$m, $\rho = 0.33$m, $g = 9.81$m/sec^2, $\phi = -\frac{\pi}{6}$rad.

Lamri Nehaoua received the B.S. degree in engineering on control and automation systems science from the University of Sétif, Algeria, in 1999 and the M.S degree in computer vision for robotics application from Clermont-Ferrand II University, France, in 2002. He is currently a PhD Student in IBISC/INRETS Laboratories, in France. His main interest is the development of vehicle and motorcycle driving simulators.